2
Thermodynamic study of an organic Rankine cycle

2.1.
System description

The traditional ORC system consists of a pump, boiler, turbine and condenser. However, in order to best describe the changes of thermodynamic states in the working fluid, the boiler has been replaced by three equivalent heat transfer zones, namely: economizer, evaporator and superheater.

Figure 3 shows a schematic diagram of waste heat recovery for power production by means of an organic Rankine cycle. Liquid from the condenser is pumped from 1 to 2 and enters the economizer, at high pressure, followed by the evaporator and the superheater. High pressure superheated vapor leaves the superheater to enter the turbine or expander, where it expands to the lower pressure of the cycle, to enter the condenser. The condensate then flows to the pump, thus closing the cycle.

Heat is transferred from the waste heat fluid to the working fluid by means of the three heat transfer zones that comprise the boiler.

It is considered that only certain data from the cycle are known in advance, and that the remainder of the waste heat fluid and working fluid thermodynamic states will depend on the operating conditions of the cycle.

The ambient temperature determines the cycle lower pressure, since the condenser will work at a pressure close to the corresponding saturation pressure relative to ambient temperature. At the turbine inlet, superheated vapor conditions are assumed and, therefore, a value of the required degree of superheating is provided as an input.

As stated before, the boiler has been substituted by three zones (each one representing a hypothetical heat exchanger): economizer[1] (ECON), evaporator (EVAP) and superheater (SUP). From Fig. 3, it can be noted that there are three different heat input rates ($\dot{Q}_{ec}, \dot{Q}_{ev}, \dot{Q}_{sh}$) and only one heat output ($\dot{Q}_{out}$) at the condenser. The total heat addition rate of the cycle ($\dot{Q}_{in}$) is the sum of the heat inputs at each of the heat exchangers:

$$\dot{Q}_{in} = \dot{Q}_{ec} + \dot{Q}_{ev} + \dot{Q}_{sh} \tag{2.1}$$

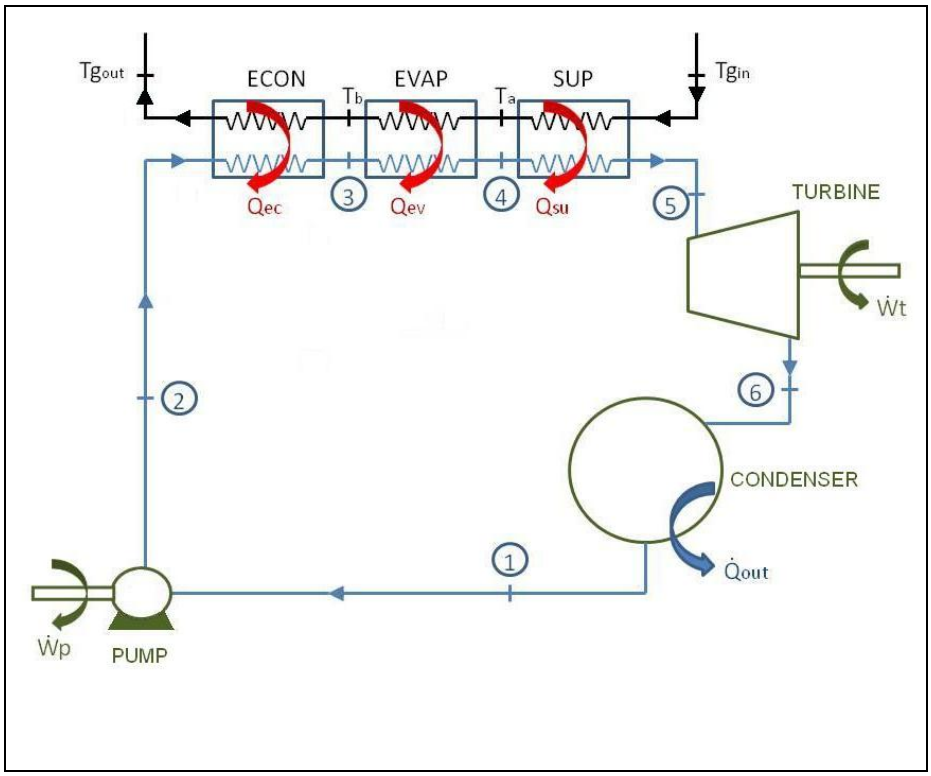

Figure 3. Diagram of waste heat recovery for power production by means of an organic Rankine cycle.

The temperature variation for the waste heat fluid as well as for the working fluid inside the boiler is shown in Fig.4, and inside the condenser in Fig.5.The waste heat fluid is cooled from Tg_{in} to Tg_{out}, which in an ORC process is much lower than in a conventional Rankine cycle because of the lower boiling point of organic fluids in comparison to water. The working fluid is preheated from T_2 to T_3, then vaporized from T_3 to T4 and, finally, superheated from T_4 to T_5.

[1] The term economizer is understood as in: [19], [28], [29]. Since the heat source is still external it should not be confused with a recuperator or regenerator.

The difference between the saturation temperature of the working fluid and the evaporator inlet temperature of the waste heat fluid is called the pinch point temperature difference.

$$\Delta T_{pinch} = T_b - T_3 \tag{2.2}$$

As shown in equation (2.2), the pinch point temperature difference can be obtained by subtracting T_3 (working fluid temperature leaving the economizer) to T_b (intermediate temperature of the heating fluid).

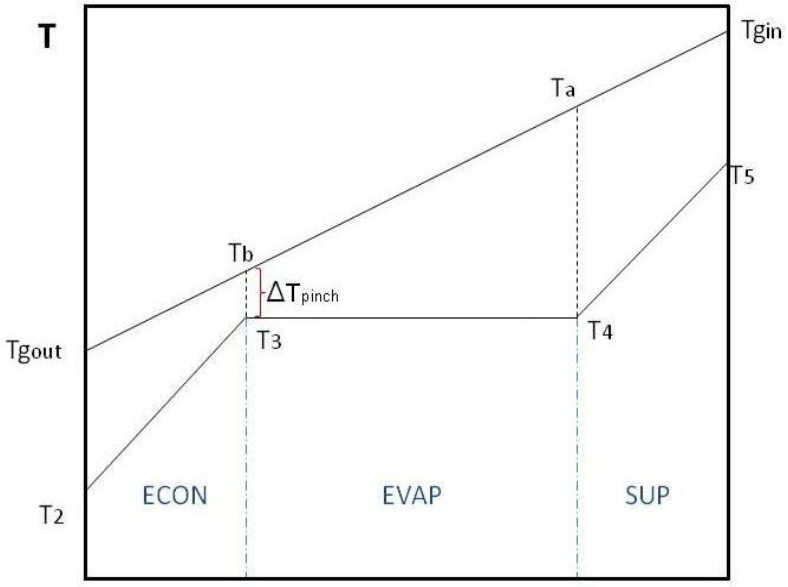

Figure 4. Temperature diagram in the boiler.

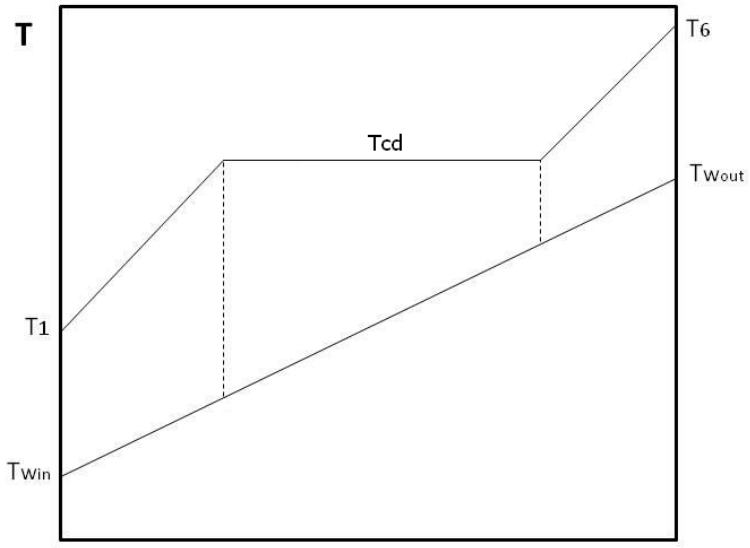

Figure 5. Temperature diagram in the condenser.

2.2.
Thermodynamic model

2.2.1.
Model approach

In order to consider the overall heat transfer and variation in the working fluid properties, the ORC system is modeled by different control volumes, representing each of the system components, as shown in Fig.6.

Mass and energy conservation equations are applied to each control volume and, together with the working fluids thermodynamic properties, form a non-linear system of algebraic equations. The solution to the system provides the rates of energy transfer and conversion of the cycle, turbine power output, mass flow rates, thermal efficiency, as well as the thermodynamic states of the working, waste heat and condenser cooling fluids.

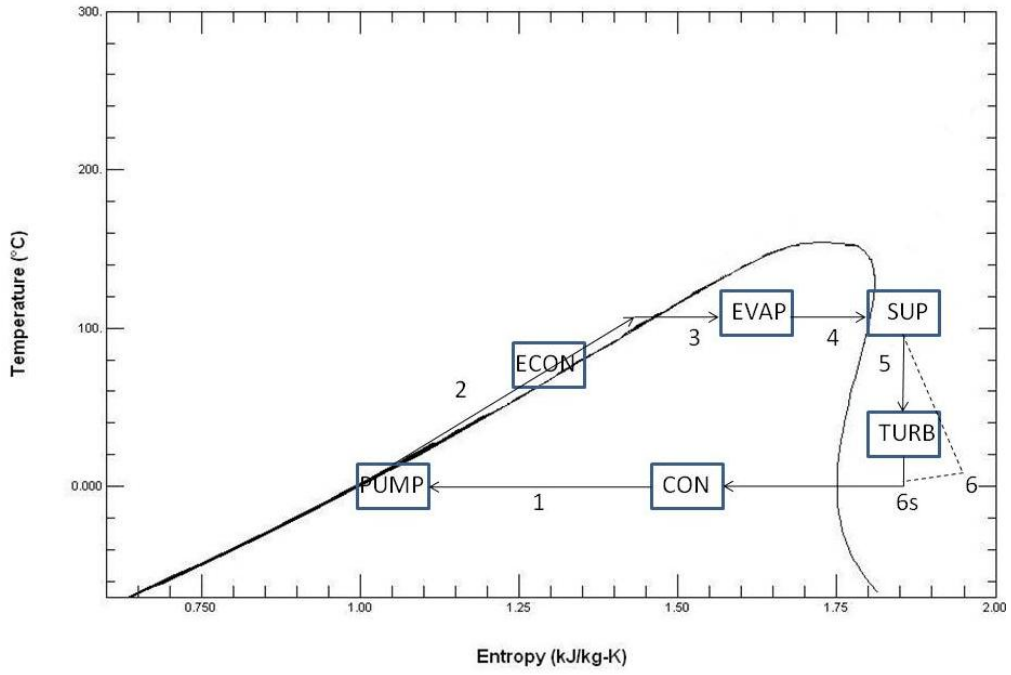

Figure 6. Control volumes in the temperature-entropy diagram of the working fluid R245fa.

2.2.2.
Model assumptions

The following assumptions were established for the thermodynamic model:

- The system is operating under steady state conditions;
- All components are considered adiabatic;
- Constant efficiencies are assumed for the pump and turbine;
- The heat exchange in the boiler is carried out in an overall counter flow configuration;
- The working fluid leaves the condenser as saturated liquid.

2.2.3.
Pump model

The power consumed by the pump is:

$$\dot{W}_p = \frac{\dot{m}_{wf}(h_{2s} - h_1)}{\eta_p} \quad (2.3)$$

where $\dot{m}_{wf}$ (kg/s) is the mass flow rate of the working fluid, h_1 and h_2 (kJ/kg) are the specific enthalpies of states 1 and 2, and η_p is the isentropic efficiency of the pump.

2.2.4.
Economizer model

The heat transfer process in the economizer can be better understood as a control volume, represented in Fig.7. The working fluid enters the economizer at temperature T_2 and leaves at T_3. Likewise, the waste heat fluid enters at temperature T_b and leaves at Tg_{out}.

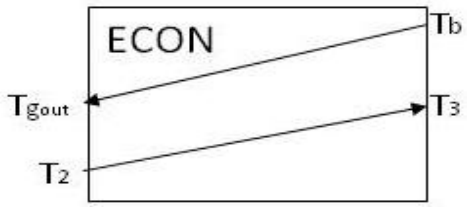

Figure 7. Control volume for the economizer.

The energy balance applied to both streams provides:

$$\dot{Q}_{ec} = \dot{m}_g c_{p,g}(T_b - T_{gout}) \quad (2.4)$$

$$\dot{Q}_{ec} = \dot{m}_{wf}(h_3 - h_2) \quad (2.5)$$

where $\dot{m}_g$ (kg/s) is the mass flow rate of the waste heat fluid, $c_{p,g}$ (kJ/kg·K) its specific heat, $\dot{m}_{wf}$ the mass flow rate of the working fluid and h_3 (kJ/kg) the specific enthalpy of state 3.

2.2.5. Evaporator model

The process in the evaporator is characterized by the phase change of the working fluid. The control volume is presented in Fig.8.

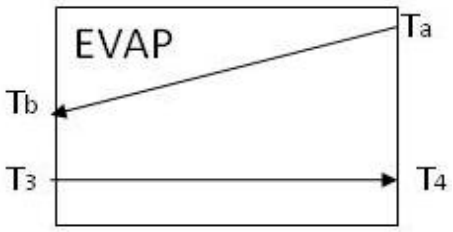

Figure 8. Control volume for the evaporator.

The energy balance and heat exchange rate equations for the evaporating zone are as follows:

$$\dot{Q}_{ev} = \dot{m}_g c_{p,g}(T_a - T_b) \quad (2.6)$$

$$\dot{Q}_{ev} = \dot{m}_{wf}(h_4 - h_3) \quad (2.7)$$

2.2.6. Superheater model

The process in the superheater is a single-phase heat exchange between the entering waste heat fluid and the working fluid in vapor phase. The control volume of the superheater is presented in Fig.9.

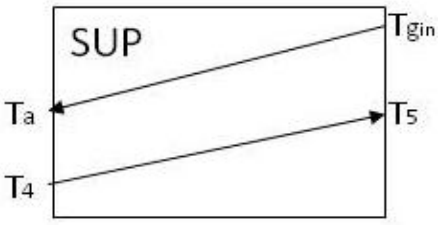

Figure 9. Control volume for the superheater.

The equations for the energy balance and heat exchange rate in the superheater are as follows:

$$\dot{Q}_{su} = \dot{m}_g c_{p,g}(T_{g,in} - T_a) \quad (2.8)$$

$$\dot{Q}_{su} = \dot{m}_{wf}(h_5 - h_4) \quad (2.9)$$

2.2.7. Expander model

The expansion of the superheated working fluid vapor in the turbine, or expander, generates shaft power. Since the expansion process is never 100% efficient in converting all of the energy available, the inclusion of the expander efficiency, η_t, is necessary.

The power generated by the expander is:

$$\dot{W}_t = \eta_t(h_{5s} - h_6) \quad (2.10)$$

2.2.8. Condenser model

The condenser receives the working fluid at superheated conditions which exchanges heat with a fluid at a lower temperature. The total heat rejection of the cycle takes place in the condenser, where the working fluid returns to liquid phase in order to enter the pump and close the cycle.

The energy balance applied to both streams yields:

$$\dot{Q}_{out} = \dot{m}_w c_{p,w}(T_{w,out} - T_{w,in}) \quad (2.11)$$

where $\dot{m}_w$ (kg/s) is the mass flow rate of the cooling water, $c_{p,w}$ (kJ/kg·K) its specific heat, $T_{w,in}$ and $T_{w,out}$ the cooling water inlet and outlet temperatures, respectively.

$$\dot{Q}_{out} = \dot{m}_{wf}(h_6 - h_1) \quad (2.12)$$

2.2.9. Thermal Efficiency

The overall thermal efficiency of the cycle is:

$$\eta_{th} = \frac{\dot{W}_t - \dot{W}_p}{\dot{Q}_{in}} \tag{2.13}$$

where $\dot{Q}_{in}$ is the sum of the heat input rates of the economizer, evaporator and superheater, $\dot{Q}_{in} = \dot{Q}_{ec} + \dot{Q}_{ev} + \dot{Q}_{sh}$, as established before.

2.3. Numerical solution

In order to solve the mathematical model of the ORC thermodynamic system, a computer program was developed, written in FORTRAN, using the Compaq Visual Fortran Professional Edition 6.5.0 compiler.

A number of subroutines were developed, granting the program modularity and making it easier for future adjustments. It also allowed for the implementation of new subroutines and models for eventually new heat transfer correlations.

The numerical solution of the mathematical model for each component of the system presents the following common characteristics:

- Equations (2.1) to (2.13) form a system of algebraic equations that give the solution.
- The thermodynamic and transport properties of the working fluids are calculated using the program REFPROP 9.0 developed by the National Institute of Standards and Technology (NIST) [41].
- The numerical solution follows a sequential structure, by solving each control volume in sequence, the following with information gathered in the previous solution.

As mentioned, only certain data inputs were considered, those available in design mode calculations. The program inputs are: type of working fluid, ambient temperature (T_{amb}), degree of superheat at expander inlet (ΔT_{sh}), pinch point differential (ΔT_{pinch}), isentropic efficiencies of the pump (η_p) and expander (η_t), mass flow rate of waste heat fluid ($\dot{m}_{hf}$) and its inlet temperature (Tg_{in}).

Figure 10 shows the input and output variables of the ORC thermodynamic model.

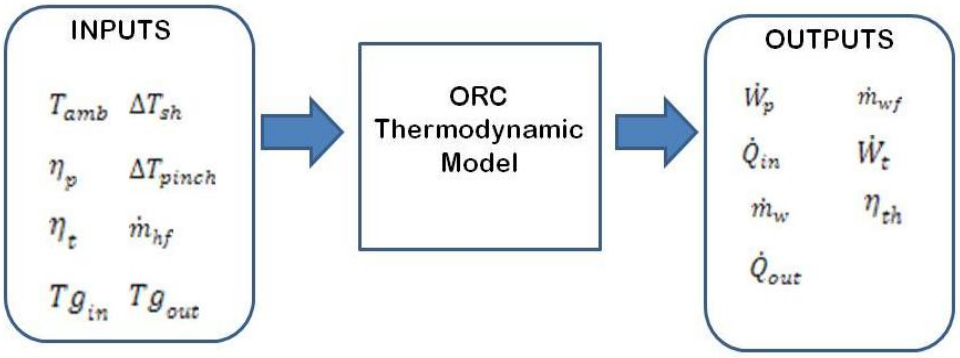

Figure 10. Solution process of the ORC thermodynamic model.

2.3.1. Solution algorithm

The numerical solution of the thermodynamic model is accomplished by following the steps below:

1. Reading of inputs.
2. From the ambient temperature and the saturation curve of the working fluid, the low pressure of the cycle is determined.
3. The properties of the working fluid at state 1 (pump inlet) are calculated from the cycle low pressure and assuming saturated liquid phase.
4. The high pressure of the cycle ranges between lower and upper limits that are calculated by adding a differential to the cycle low pressure until it reaches 90% of the working fluids critical pressure, in order for the process not to reach a transcritical condition.
5. Considering the efficiency of the pump and using the high pressure of the cycle, the properties of state 2 (pump outlet) are calculated.
6. State 3 (economizer outlet) properties are calculated with the high pressure of the cycle and assuming, by definition, saturated liquid phase at the economizer outlet.
7. The properties of state 4 (evaporator outlet) are calculated from the high cycle pressure and heat gained from the waste heat fluid.

8. The working fluid properties of state 5 (superheater outlet) are calculated from the prescribed degree of superheat and the cycle high pressure.
9. State 6 (expander outlet) properties are calculated by considering the efficiency of the expander and the low pressure of the cycle.
10. With the thermodynamic states at each of the control volumes the output variables are calculated.

2.3.2. Working fluids

In order to employ the model to a wider range of ORC applications, the study considered five different pure working fluids, divided into two groups, according to their range of applicability. Working fluids are limited by the temperatures and pressures they will endure, for them not to exceed their thermal stability limit and compromise their properties. The two groups considered for ORC applications depend on the type of heat source, thus fluids R245fa and R123 are more suitable for recovering from gaseous heat sources (e.g. Diesel engine exhaust gases), whereas R1234yf, R1234ze and R134a are more suitable to recover heat from liquid sources (e.g. geothermal hot water). Table 1 shows the properties of the different working fluids considered, divided for their appropriate heat recovery application.

Table 1. Properties of the different working fluids [41].

		Gaseous heat source		Liquid Heat Source		
		R245fa	R123	R1234yf	R1234ze	R134a
Molar mass (kg/kmol)		134.05	152.93	114.04	114.04	102.03
Triple point temperature (K)		171.05	166	220	168.62	169.85
Critical Point	Temperature (K)	427.2	456.83	367.85	382.52	374.21
	Pressure (MPa)	3.64	3.6618	3.38	3.63	4.0593
	Density (kg/m³)	517	550	475.55	489.24	511.9
Normal boiling point (K)		288.05	300.97	243.7	254.2	247.08

2.3.3. Validation of the thermodynamic model

The simulation results were validated against design data obtained from Aneke et al. [42]. The data is from the Chena Geothermal ORC Power Plant in the city of Chena, Alaska.

Table 2. Validation of the thermodynamic model with real data from the Chena Geothermal Power Plant [42].

Parameter	Chena Geothermal ORC power plant data	Simulation input data	
Geothermal fluid mass flowrate (kg/s)	33.39	33.39	
Geothermal fluid temperature (°C)	73.33	73.33	
Cooling water mass flowrate (kg/s)	101.68	101.68	
Cooling water source temperature (°C)	4.44	4.44	
Working fluid	R134a	R134a	
Turbine efficiency	0.8	0.8	
Turbine inlet pressure (bar)	16	16	
Turbine outlet pressure (bar)	4.39	4.39	
Gross generator power (kW)	250	250	
Pump power (kW)	40	40	
		Simulation result	**% Relative error**
Geothermal exit temperature (°C)	54.44	54.93	0.89
Cooling water exit temperature (°C)	10	9.95	0.50
Working fluid mass flowrate (kg/s)	12.17	11.88	2.38
Thermal Efficiency	0.08	0.084	4.8
Boiler heat transfer rate (kW_{th})	2580	2555.91	0.94
Condenser heat transfer rate (kWth)	2360	2356.69	0.14

The comparison between simulation results and plant design data are presented in Table 2. The results from the simulation matched the real plant data accordingly and, therefore, it can be inferred that the model is suitable for the calculation and sizing of an ORC plant using a similar type of waste heat.

2.3.4.
Thermodynamic model results

As stated in the solution algorithm, the program calculates different high cycle pressures; this allows for the determination of the optimum operating condition of the cycle for certain given inputs. On Figs. 11 through 14, the results of the calculated net power output and thermal efficiency against reduced high pressure, $P_r = \frac{P}{P_{crit}}$, are shown.

Figure 11 shows the net power output for R245fa and R123, the fluids considered for the recovery of waste heat from a gaseous source. The net power output increases jointly with the high pressure of the cycle for both working fluids, reaching an asymptote and, in the case of R123, slightly decreasing. This can be understood since the working fluid gains less energy as it approaches the critical pressure, showing that there is an optimum working pressure. Under the same working conditions, R245fa proved to have a better performance. Figure 12 shows the thermal efficiency of these two working fluids against the reduced pressure. As shown, the efficiency is limited to just fewer than 23%. Working fluid R245fa demonstrated to have a better thermal efficiency for the studied case.

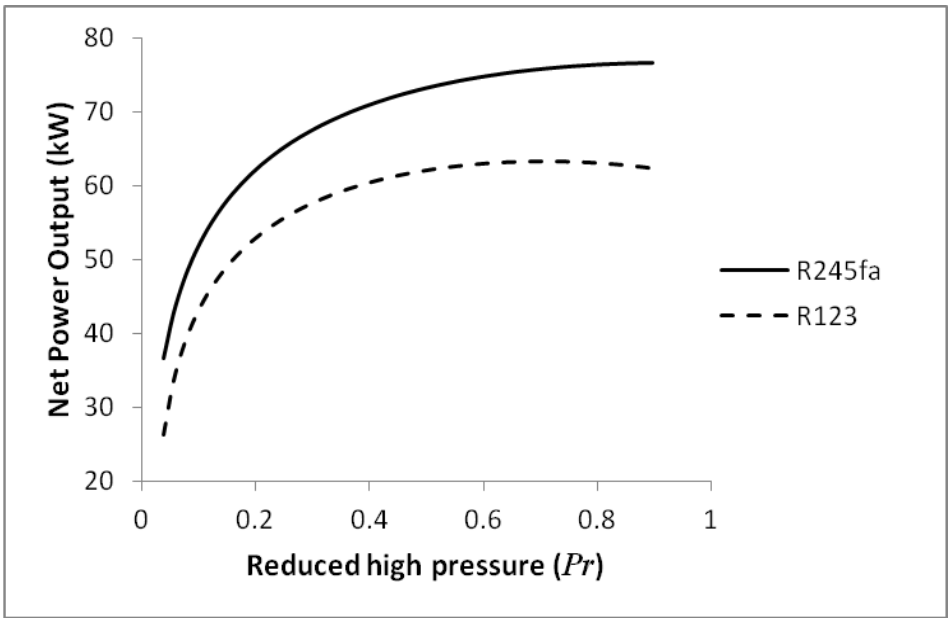

Figure 11. Net Power output for R245fa and R123 at (T_{amb}=298K, ΔT_{sh}=10K, ΔT_{pinch}=5K, $\dot{m}_{hf}$=3kg/s, Tg_{in}=460K)

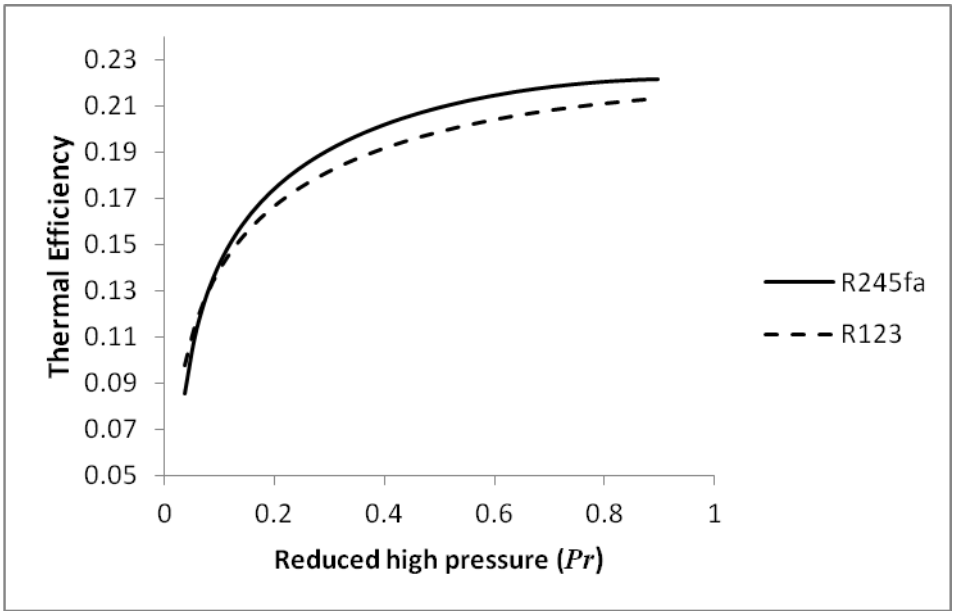

Figure 12. Thermal efficiency for R245fa and R123 at (T_{amb}=298K, ΔT_{sh}=10K, ΔT_{pinch}=5K, $\dot{m}_{hf}$=3kg/s, Tg_{in}=460K)

Figure 13 shows the net power output of R134a, R1234yf and R1234ze, the fluids considered to recover waste heat from a liquid source. All working fluids show an increase in net power output along with the high pressure of the cycle. R134a and R1234ze presented the best results and a minimal difference between them. R1234yf had the least power output for the prescribed working conditions.

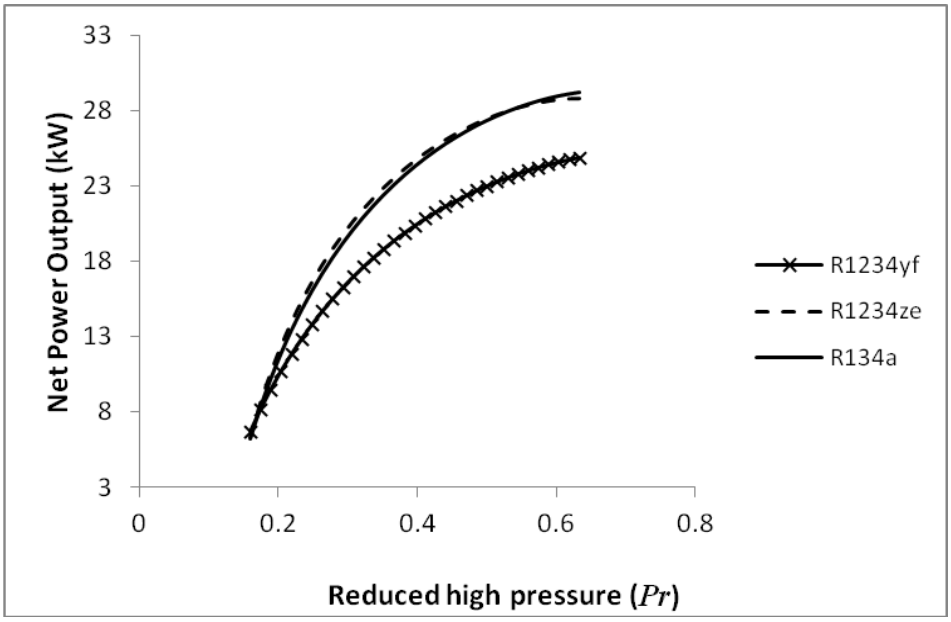

Figure 13 Net Power output for R1234yf, R1234ze and R134a at (T_{amb}=298K, ΔT_{sh}=5K, ΔT_{pinch}=2K, $\dot{m}_{hf}$=10kg/s, Tg_{in}=350K)

Figure 14 shows the thermal efficiencies of R134a, R1234yf and R1234ze. For the imposed conditions, it was found, from computed results, that these working fluids could only effectively work at less than 70% of their critical pressures. It is shown that all thermal efficiencies increase as the high pressure of the cycle rises. Working fluid R1234ze showed the best thermal efficiency, followed by R134a and R1234yf.

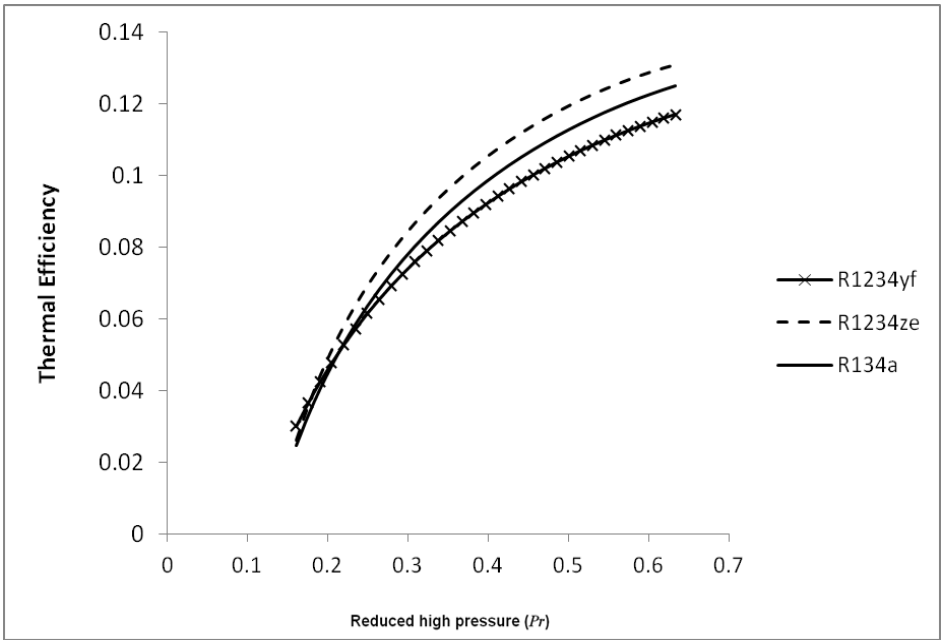

Figure 14. Thermal efficiency for R1234yf, R1234ze and R134a at (T_{amb}=298K, ΔT_{sh}=5K, ΔT_{pinch}=2K, $\dot{m}_{hf}$=10kg/s, Tg_{in}=350K)